Aeolian Research 34 (2018) 35–48

Contents lists available at ScienceDirect

Aeolian Research

journal homepage: www.elsevier.com/locate/aeolia

Measurement and modeling of the spatiotemporal dynamics of beach surface moisture content

Phillip P. Schmutz[a,*], Steven L. Namikas[b]

[a] Department of Earth and Environmental Science, University of West Florida, Pensacola, FL 31514, USA
[b] Department of Geography and Anthropology, Louisiana State University, Baton Rouge, LA 70803, USA

ARTICLE INFO

Keywords:
Beach surface moisture
Beach hydrology
Groundwater fluctuations
Capillary transport
Evaporation

ABSTRACT

The spatiotemporal dynamics of surface moisture exert a significant influence on the operation of aeolian transport systems at many beaches. However, we currently lack the detailed understanding of variability in surface moisture required to incorporate it into aeolian models. This problem is addressed here through direct measurements and simulation modeling of beach surface moisture over a twelve-day period, and through quantification of the relative contributions of evaporation, condensation and groundwater inputs to surface moisture. It was found that the beach surface can be characterized spatially in terms of three moisture zones: a consistently dry zone (< 3%); a variable zone (3% to saturation); and a consistently wet zone (> 40%). The relative influence of groundwater inputs was found to decrease moving landward, as the depth of the water table increased and the amplitude of tidally-induced water table fluctuations decreased. The critical pressure head (groundwater depth) at which evaporation begins to impose a demonstrable influence on surface moisture variability was found to be 90–100 cm. Temporally, beach surface moisture is a function of the lunar tidal cycle at longer-term time scales (weekly), and diurnal tidal and evaporation cycles. A numerical model was used to simulate capillary transfers of moisture from the water table to the surface, and moisture losses due to evaporation. The model was found to reliably replicate the measured spatiotemporal variability in surface moisture. In the dry zone, where most aeolian transport would be expected to occur, simulated moisture contents were typically within ± 0.2% of measured volumetric contents.

1. Introduction

It is generally acknowledged that the beach hydrological system is a critical parameter influencing a broad range of environmental phenomena including earth-atmospheric energy fluxes, beach stability, nutrient cycling, water purification, coastal water resource budgets, and interstitial biological activity (e.g., Hesp, 1991; McLachlan, 1989; Famiglietti et al., 1998; Barrilleaux and Grace, 2000; Horn, 2002; Abu-Hamdeh, 2003; Chen and Hu, 2004; Legates et al., 2010; Vicinanza et al., 2010). The cohesive forces induced by the presence of moisture at the sediment surface are often cited as a factor influencing aeolian transport, one that acts to limit the frequency and magnitude of transport events (e.g., Namikas and Sherman 1995; Cornelis and Gabriels, 2003; Wiggs et al., 2004a,b; Davidson-Arnott et al., 2008; Rotnicka, 2013; de vries et al., 2014; Haehnel et al., 2014; Poortinga et al., 2014; Edwards and Namikas, 2015; Hoonhout and de Vries, 2016). Thus, beach surface moisture can exert an important control on coastal dune development. Although a number of studies have explored this influence (e.g., Bauer and Davidson-Arnott, 2002; Aagaard et al., 2004; Bauer et al., 2009; Houser, 2009; Lynch et al., 2016; Hoonhout and de Vries, 2017), the applicability of theoretical aeolian transport rate models to the real world remains substantively handicapped by our inability to accurately describe spatiotemporal beach surface moisture dynamics.

A number of studies have provided data regarding the variability in surface moisture in beach environments (e.g., Atherton et al., 2001; McKenna Neuman and Langston, 2003; Wiggs et al., 2004a; Yang and Davidson-Arnott, 2005; Davidson-Arnott et al., 2005; McKenna Neuman and Langston, 2006; Zhu, 2007; Davidson-Arnott et al., 2008; Bauer et al., 2009; Namikas et al., 2010; Brakenhoff, 2015). These data clearly indicate that surface moisture content varies considerably in both space and time, both at a given beach and from beach to beach. The available database, however, is insufficient to provide for a general characterization of beach moisture variability of sufficient detail to support realistic aeolian transport or sediment budget modeling. This is in large part due to the complex and variable nature of the suite of

* Corresponding author.
E-mail addresses: pschmutz@uwf.edu (P.P. Schmutz), snamik1@lsu.edu (S.L. Namikas).

https://doi.org/10.1016/j.aeolia.2018.08.001
Received 26 May 2018; Received in revised form 9 August 2018; Accepted 9 August 2018

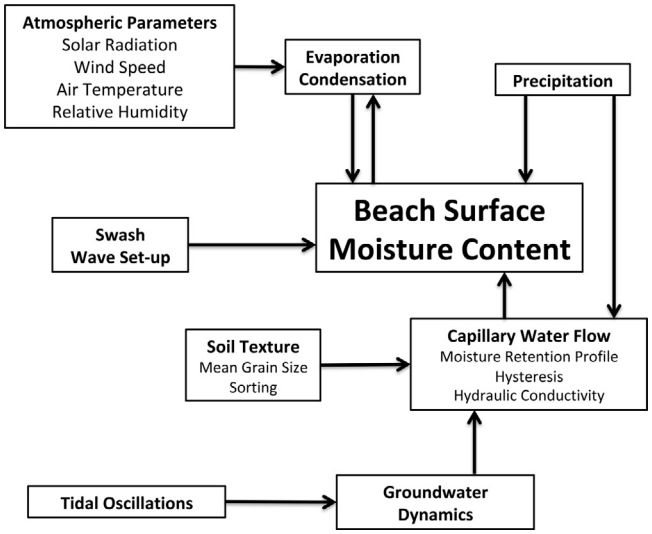

Fig. 1. Key processes and parameters that control beach surface moisture dynamics.

hydrological, meteorological and sedimentary parameters [e.g., precipitation, tidal oscillations, groundwater flow, capillary transport, evaporation, condensation, sediment size, sorting, porosity, hydraulic conductivity, etc.], which regulate beach surface moisture (Fig. 1). Although the importance of some of these parameters has been identified in previous studies (e.g., Atherton et al., 2001; Zhu, 2007; Namikas et al, 2010; Brakenhoff, 2015), our ability to model the beach hydrological system in the context of its control on surface moisture remains limited. This issue must be resolved to allow the development of realistic models of surface moisture variability, and their ultimate incorporation into aeolian transport budget and dune development models.

This study documents and models several key components of the beach hydrological system (tidal oscillations, water table fluctuations, capillary transport, evaporation, condensation), and their influence on spatiotemporal variability in surface moisture content. The specific research objectives are to: 1) measure spatiotemporal variability in surface moisture across a spring-neap tidal cycle; 2) link measured surface moisture variability to contemporaneously monitored controlling processes/parameters; and 3) construct a physically-based numerical model capable of reproducing the measured variability in beach surface moisture over both space and time.

2. Methods

2.1. Study site

The field experiment was conducted over 12 days (January 18–29), at Padre Island National Seashore on the central Texas coast (Fig. 2). The native quartz sediment is well sorted with a mean grain size of about 0.14 mm. The beach environment at the time of the study was comprised of a gently sloping berm extending about 50 m from the foredune to the berm crest. Scattered, small embryo dunes extended approximately 5–10 m onto the beach from a well-established 2–3 m high foredune. The central Texas coast experiences a micro-tidal range (typically less than one meter), with mixed but predominately diurnal tidal cycles (Weise and White, 1991).

2.2. Field methods

2.2.1. Surface moisture measurement

To map spatial and temporal surface moisture patterns, a grid of measurement points was established across the beach (Fig. 3). The moisture grid comprised of 12 alongshore lines sequentially designated as L1 to L12. The lines were spaced at 2.5 m to 5 m intervals in the cross-shore direction, and each line consisted of five measurement points spaced 5 m in the alongshore direction. Measurement of surface moisture contents were performed using a Delta-T Theta soil moisture probe, modified to limit measurement depth to 1.0 cm (Tsegaye et al, 2004; Yang and Davidson-Arnott, 2005; Schmutz and Namikas, 2011). Grid moisture contents were measured six times per day (dawn, mid-morning, solar noon, mid-afternoon, sunset, and middle night). The sampling schedule was based on consideration of expected rates of change in surface moisture, as well as the desire to minimize the small but cumulative surface disruptions resulting from probe insertion. During high tide, swash process often submerged measurement lines L10-L12 (seaward-most lines). Therefore, measurements were not collected during these times as the beach surface sediment was presumed saturated (45% content by volume – determined through laboratory analysis from this study and past research conducted by the authors at the field site).

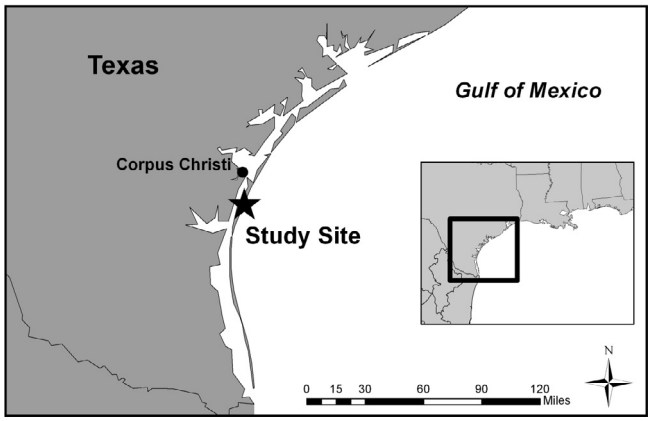

Fig. 2. Location of Padre Island National Seashore field site.

2.2.2. Water table depth and tidal elevation measurements

Water table depth was monitored using four groundwater wells (designated W1 to W4 on Fig. 3) that were installed on lines L1, L4, L6 and L9. A pressure transducer (PT) (Global Water WL400 or KPSI 730) was installed in each well and monitored at five minute intervals to document water table fluctuations. Tidal oscillation was initially monitored using a Global Water WL400 pressure transducer installed in the nearshore zone 50 m seaward of the berm crest. However, this instrument failed on the second day of the experiment so all tide data utilized in this study was obtained from a National Oceanic and Atmospheric Association (NOAA) tide gauge located at Bob Hall Pier, about 10 km north of the study site. Previous work by Zhu (2007) has demonstrated that data from this NOAA gauge correlate closely with pressure transducer measurements at the study site.

2.2.3. Potential evaporation and atmospheric measurements

Potential evaporation rates were measured using a standard National Weather Service Class A evaporation pan (Fig. 3) equipped with a digital depth sensor (readable to 0.01 mm) mounted within a stilling well. Measurements of the evaporation pan water elevation were recorded six times per day, concurrent with each set of moisture grid measurements.

Wind speed and direction were measured using a set of three RM Young cup anemometers at elevations of 1.0, 2.0 and 5.0 m above the beach surface, and a Qualimetrics Micro Response wind vane at the top of the weathermast (5.5 m) respectively. Air temperature and relative humidity were monitored using two Campbell Scientific HMP45C temperature/humidity transmitters installed on the mast at elevations of 1 m and 5 m. Precipitation was monitored using a Texas Electronics

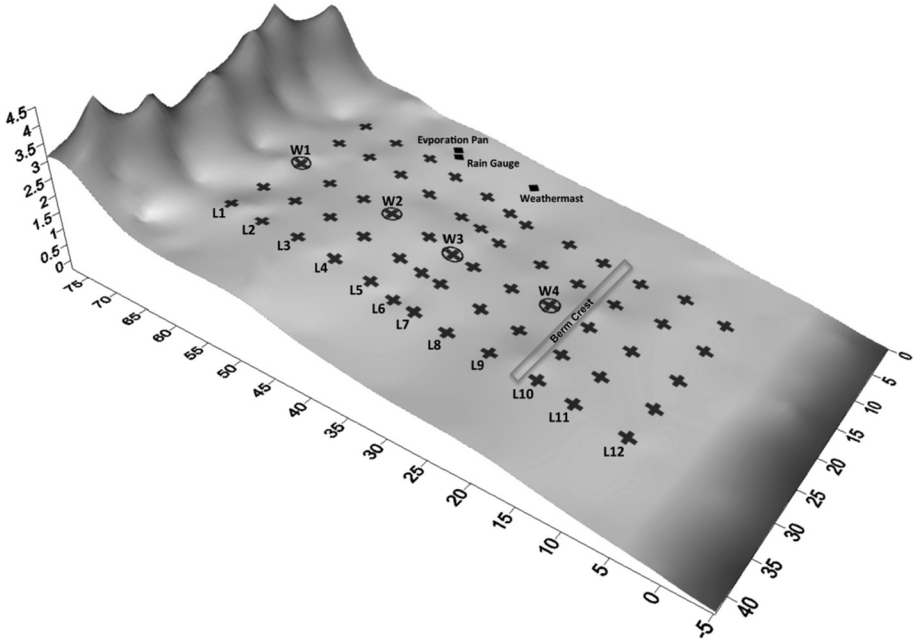

Fig. 3. Three-dimensional topographic overview of study area showing the surface moisture measurement lines (L1–L12), groundwater wells (W1–W4) and sensor locations. Cross-shore distance is relative to mean sea level position (MSL = 0). Dune toe is approximately 65 m in cross-shore distance from MSL.

TE525 rain gauge (Fig. 3), although no rainfall occurred during the experiment. All weather instruments were cabled to a Campbell Scientific CR3000 data logger and the data were logged at 5 min intervals.

2.3. Data analysis and model

2.3.1. Hysteretic capillary flow model (HCFM)

Surface moisture contents were simulated using a HCFM to represent capillary transfer from the water table to the surface. Model simulations were employed using the HYDRUS-1D program developed by Šimůnek et al. (1998). The HYDRUS-1D program calculates hysteretic water flow in a sediment profile derived via the hysteretic function originally developed by Scott et al. (1984), and later modified by Vogel et al. (1996).

The modeling procedure requires that both the main drying and wetting boundary moisture retention curves ($\theta^d(h)$ and $\theta^w(h)$) and the unsaturated hydraulic conductivity curves ($K^d(h)$ and $K^w(h)$) of the sediment are known. The moisture retention and unsaturated hydraulic conductivity curves are thus described as follows:

$$\theta^d(h) = \theta_s + \alpha_\theta[\theta^{d*}(h) + \theta_r]$$
$$\theta^w(h) = \theta_r + \alpha_\theta[\theta^{w*}(h) + \theta_s] \quad (1)$$

and

$$K^d(h) = \alpha_K K^{d*}(h)$$
$$K^w(h) = K_r + \alpha_K K^{w*}(h) \quad (2)$$

where θ^d is the volumetric water content of the main drying branch, θ^w is the volumetric water content of the main wetting branch, h is the water pressure head (expressed as negative or tension pressure head), θ_s is the saturated water content, equivalent to porosity, θ_r *is* the residual water content, defined as the moisture content when the gradient ($d\theta/dh$) becomes zero; K^d is the unsaturated hydraulic conductivity of the main drying branch, K^w is the unsaturated hydraulic conductivity of the main wetting branch, α_θ and α_K are independent scaling factors for water content and hydraulic conductivity, respectively; K_r is the residual hydraulic conductivity, defined as the conductivity when the gradient (dK/dh) becomes zero. The model represents changes in the drying and wetting branch hydraulic properties of a given soil profile through a set of scaling transformations (θ^{d*}, θ^{w*}, K^{d*}, K^{w*}) based on Miller and Miller's (1956) 'similar media concept' (Scott et al., 1984).

Evaporation dynamics are incorporated into the HYDRUS model via a system-dependent condition at the upper boundary obtained via a percentage of the total daily value of the evaporation flux depending upon the hour of measurement:

$$E_{ph}(t) = 0.24\bar{E_p} \quad t < 0.25d,\ t > 0.75d$$
$$E_{ph}(t) = 2.75\bar{E_p} \quad t \in 0.25d,\ 0.75d \quad (3)$$

where E_{ph} is the Hydrus derived potential evaporation rate, t is time at measurement, $\bar{E_p}$ is the daily value of potential evaporation, and d is 24 h time. HYDRUS-1D assumes that evaporation flux values between 0–6 a.m. and 18–24 p.m. represent 1% of the total daily value evaporation flux. For a detailed description of the hysteretic capillary water flow model and the implementation of evaporation into the model see Šimůnek et al. (1998).

2.3.2. Moisture retention curves and hydraulic conductivity

The moisture retention and unsaturated hydraulic conductivity curves were determined using the soil hydraulic functions proposed by van Genuchten (1980):

$$\theta(h) = \theta_r + \frac{\theta_s - \theta_r}{[1 + (\alpha h)^n]^m} \quad (4)$$

$$K(h) = K_s\Theta^\lambda[1-(1-\Theta^{1/(m)})^m]^2 \quad (5)$$

where h is the water pressure head (expressed as negative pressure head), θ_s is the saturated water content, θ_r *is* the residual water content, α and n are empirical parameters, m = 1-(1/n), Θ is the effective degree of saturation, K_s is the saturated hydraulic conductivity, and λ is a pore connectivity parameter shown by Mualem (1976) to have a value of 0.5. To designate the main drying and wetting boundary moisture retention and unsaturated hydraulic conductivity curves, the function parameters θ_r, θ_s, α, n, m, and K_s are denoted with superscripts d and w to indicate either a drying or wetting curve, respectively. The surface moisture measurements collected along the grid lines that incorporated the groundwater wells ranged from nearly dry to saturated, and thus provided the necessary data for construction of the main drying and wetting moisture retention curves and the unsaturated hydraulic

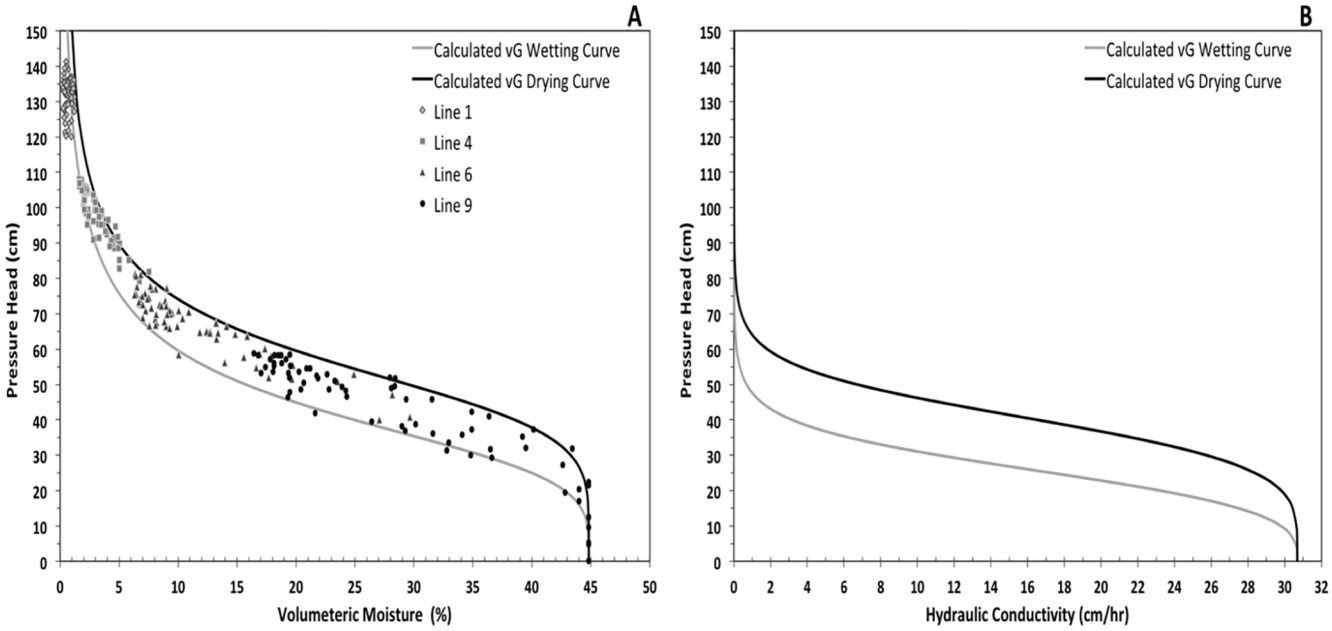

Fig. 4. (A) Measured volumetric moisture contents and the calculated van Genuchten (1980) boundary wetting and drying moisture retention curves, and (B) the calculated van Genuchten (1980) boundary wetting and drying unsaturated hydraulic conductivity curves. The pressure head associated with each measurement point in Lines 1, 4, 6, and 9 is equivalent to the height of the ground surface above the water table.

conductivity curves (Fig. 4).

2.3.3. Soil surface evaporation model

Numerous studies have illustrated that actual soil surface evaporation dynamics do not consistently approximate the potential evaporation rate (e.g. Holmes, 1961; Monteith, 1965; Ritchie, 1972; Idso et al., 1974; Monteith, 1981; Paralange and Katul, 1992; Wilson et al., 1997; Aydin et al., 2005). However, the direct measurement of soil surface evaporation is extremely difficult and not possible without substantially impacting other components of the system (e.g., through use of a lysimeter) that are of critical interest to this study. Previous work by Mahfouf and Noilhan (1991) established a model to calculate bare (i.e., actual) soil surface evaporation (E_b). The authors established E_b as a function of the potential evaporation rate with adjustments to incorporate vegetation and surface moisture:

$$E_b = (1-\sigma_v)\beta E_p \tag{6}$$

where σ_v is the ratio of vegetation cover to bare ground (equal to 0 for a bare soil such as beach sand), E_p is the potential evaporation, and β is the moisture availability, given as:

$$\beta = \begin{cases} \frac{\theta-\theta_r}{\theta_s-\theta_r}, & \theta < \theta_{fc} \\ 1, & \theta \geq \theta_{fc} \end{cases} \tag{7}$$

where θ_r is the residual water content, θ_s is the saturation water content, θ_{fc} is the field capacity water content, and θ is the measured water content.

2.3.4. Groundwater elevation interpolation

Groundwater elevation was directly measured only at L1, L4, L6, and L9, so water table depths at other lines had to be interpolated from these data. The interpolation approach developed by Zhu (2007) was employed for this purpose. This approach utilizes the linearized one-dimensional Boussinesq equation incorporating a sloping beach to include the effect of a moving shoreline. The linearized one-dimensional form of the Boussinesq equation is given as follows:

$$\frac{\partial z}{\partial t} = \frac{K_s H_0}{n_e}\frac{\partial^2 z}{\partial x^2} \tag{8}$$

with the boundary conditions:

$$z(0, t) = H_0 + \eta_{tide}(t) \quad x = 0 \tag{9}$$

$$\frac{\partial z}{\partial t} = \frac{\partial z}{\partial x} \to 0 \quad x \to \infty \tag{10}$$

where t is time (s), z is the elevation of the water table (m), n_e is specific yield (dimensionless), η_{tide} (t) is the elevation change of tide at time t, x is horizontal distance landward (m), K_s is the saturated hydraulic conductivity (m/s), and H_0 is mean water level [function of mean sea level]. The main assumption in using Eq. (8) is that groundwater flow in a shallow aquifer is that horizontal flow dominates over vertical flow. A number of field studies (e.g., Baird et al., 1998; Raubenheimer et al., 1999) describing tidal groundwater flow on beaches underlain by relatively impermeable material support this assumption.

To incorporate the effect of a moving shoreline, Zhu (2007) expanded upon the concept put forth by Li et al. (2000), whom replaced the 'x' term in the linearized Boussinesq equation (Eq. (8) with the term 'f':

$$f = x - \frac{\eta_{tide}(t)}{\tan\beta} \tag{11}$$

where β is the foreshore slope angle. Li et al. (2000), however, assumed the moving boundary of the shoreline to equal the range of tide oscillation dismissing the influence of wave setup, which increases not only the mean water surface in the foreshore but also the horizontal range of shoreline (i.e. the seaward boundary of beach groundwater). To incorporate wave setup Zhu (2007) included a wave setup angle term (α) into the 'f' term of Li et al. (2000),

$$f = x - \frac{\eta_{tide}(t)}{\tan\beta - \tan\alpha} \tag{12}$$

where Zhu (2007) defined as $\tan\alpha = 0.232 \tan\beta$.

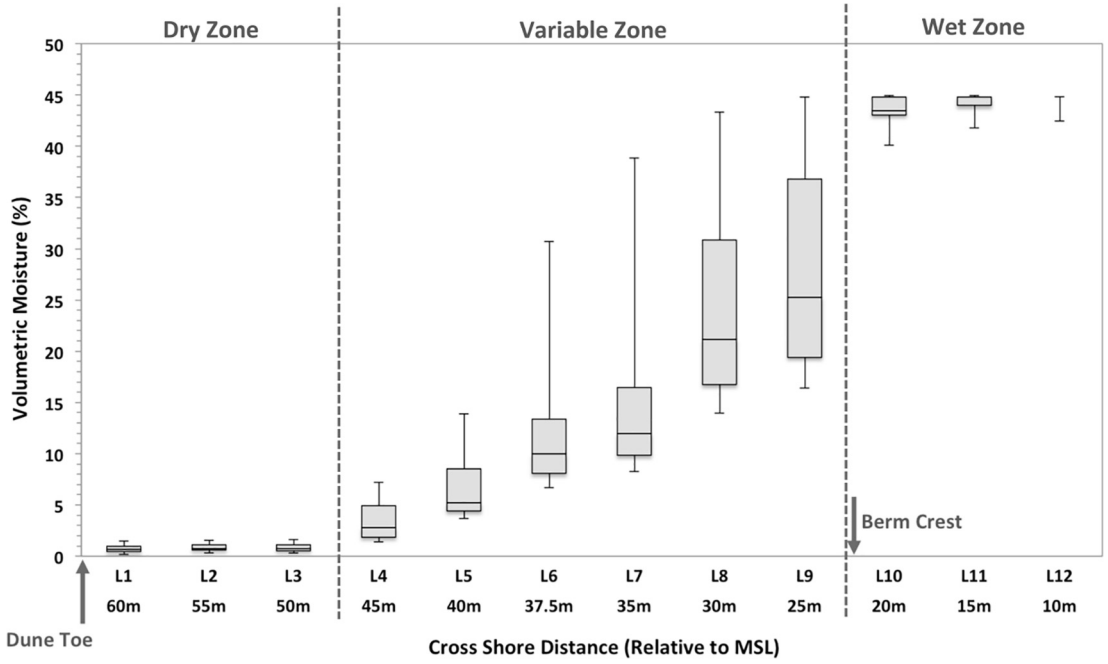

Fig. 5. Box-Whisker plot of surface moisture content for each measurement line. The whiskers bounding each box indicate the minimum and maximum recorded values. The boxes are bounded by the lower and upper quartiles of all records, and the line in each box indicates the median moisture content. Arrows mark spatial locations of dune toe and berm crest.

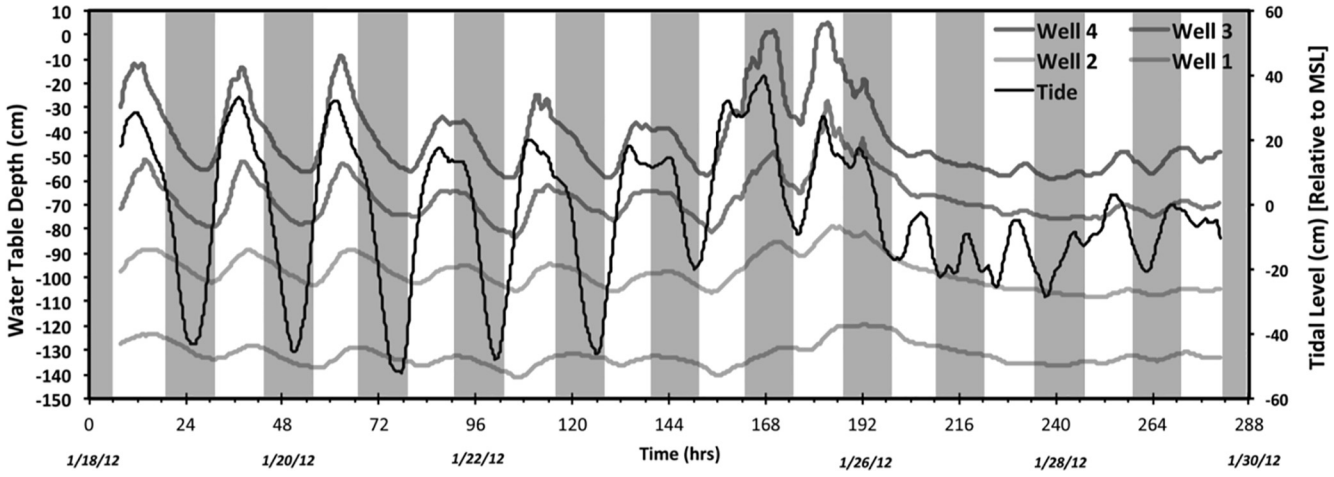

Fig. 6. Time-series of water table depth at each well and tidal elevation. Dark and light bars correspond with day and night.

3. Results: Field measurements

3.1. Spatial variation in surface moisture

The volumetric moisture measurements collected at each of the alongshore grid lines are summarized in Fig. 5. On this plot, the whiskers indicate minimum and maximum moisture content for a given line, while the boxes are bounded by the upper and lower quartiles and the line within each box plot indicates the median moisture content for that line. The vertical extent of the boxes thus provides a visual indicator of the typical variability in measured moisture content. Based on the magnitude of this variability, the beach can be characterized in terms of three distinct surface moisture zones, as originally described in Namikas et al. (2010): 1) a low-variability, consistently high moisture content 'wet zone' on the upper foreshore (L10–L12); 2) a high variability, decreasing moisture content 'variable zone' extending from the berm crest to within about 10–15 m of the dune toe (L4–L9); and 3) a low variability, consistently low moisture content 'dry zone' of about 10–15 m width fronting the dune toe (L1–L3).

The wet zone on the upper foreshore experienced very high surface moisture levels (> 40%) that consistently remained at or very near saturation. In this zone the beach surface was often submerged by swash at high tide, causing saturation. During low tide this portion of the foreshore was fully subaerial. However, the surface sediment still remained at or near saturation due to the capillary fringe, the near-saturated sediment layer above the water table (Horn, 2002). At the study site the height of the capillary fringe during low water levels (i.e., during the drying cycle) was approximately 30 cm (see Fig. 4A, VG-Drying Curve) and the depth to the water table was typically less than 45 cm. As a result, surface moisture contents across the foreshore remained quite high and exhibited little variability.

The variable zone extends landwards from the berm crest to within about 10–15 m of the dune toe. Measured surface moisture contents in this zone ranged from nearly dry (3%) to saturated (45%), and consistently decreased in the landward direction. In this zone the beach slopes gently upward in the landwards direction, which contributes to

increasing water table depth and decreasing surface moisture content. The water table depth ranged from a minimum of less than 5 cm at the seawards boundary of the zone during high tide, to a maximum of about 80 cm at the landward boundary associated with low tide (see Fig. 6, Wells 2, 3 and 4). Note that pressure head values in this zone primarily fall in the 'flatter' portion of the moisture retention profile (Fig. 4A). As a result, the vertical gradient in moisture content below the surface is quite steep, and therefore small fluctuations in the water table can produce large changes in surface moisture content. Accordingly, this zone consistently exhibits the largest variability in surface moisture content.

Lastly, a consistently stable dry zone (moisture content < 3%) is found along the back beach, extending about 10–15 m seaward from the foredune toe. This condition can be attributed to greater water table depths (> 100 cm) and to the relatively small amplitude of tidally-induced water table fluctuations (see Fig. 6, Well 1). The beach surface in this zone is located in the near-vertical, steep end of the moisture retention profile (Fig. 4A) thus surface moisture remains very stable producing minimal change in moisture content.

3.2. Temporal variation in surface moisture

The observed temporal variations in groundwater fluctuations and surface moisture content (Figs. 6 and 7) can be largely attributed to the lunar spring/neap and diurnal tidal cycles, which regulate the timing and amplitude of beach water table fluctuations (Baird and Horn, 2006), as well as diurnal cycles in evaporation and condensation. Several temporal patterns in beach surface moisture content are evident in the data, over both long-term (multi-day) and short-term (daily) periods.

3.2.1. Long-term (Multi-day) variations

Examination of the tidal, water table and moisture content fluctuations in the variable zone (Figs. 6 and 7) indicates the occurrence of four relatively distinct fluctuation regimes during the study period. These include an initial period of large amplitude fluctuations associated with the spring tide portion of the lunar tidal cycle (hours 8–80). This was followed by a period of decreasing fluctuation amplitude as the tidal cycle moved toward neap tide (hours 80–158). The transition to neap tide conditions was interrupted by a spike in water elevation that persisted for about 2 diurnal cycles (hours 158–209). Based on the field observations, we attribute this anomalous increase in both water elevation and surface moisture content to wind and wave set-up induced by strong onshore winds (hours 160–190) and relatively large wave heights. Finally, a period of minimal fluctuation amplitude occurred in association with neap tidal conditions (hours 209–281).

Fig. 8 illustrates box and whisker plots of beach surface moisture for each beach moisture zone, subdivided into the four time periods identified above (i.e., spring tide, decreasing tidal range, wind/wave set-up, and neap tide). This figure demonstrates that the three moisture zones exhibit quite different responses to changes in the tidal fluctuation regime. Changes in the magnitude of surface moisture variability are most evident in the central portion of the variable zone (L5-L8), where variability decreases dramatically between spring and neap tide conditions. Both the wet zone (L10–L12) and dry zone (L1–L3) remained relatively stable, with only small changes in moisture content median or range regardless of variation in the amplitude of water elevation fluctuations. The only substantial exception occurred in the wet zone during the period of set-up induced high water levels. Water levels during this period were high enough that lines 10–12 were submerged for almost the entire period so that surface moisture remained at saturation even at low tide.

3.2.2. Short-term (Diurnal) variations

Surface moisture content at all lines displayed well-defined diurnal cycles throughout the field experiment (Fig. 7). The variable and wet zones both typically experienced peak surface moisture levels in mid-afternoon to early evening and minimum levels near dawn. The timing of these cycles corresponded closely to tidal elevation (Fig. 9a), illustrating the influence of the tide as a control of surface moisture in these zones. The duration of peak surface moisture contents is much longer for the wet zone due to the occurrence of swash inundation (Fig. 7c).

In the dry zone the diurnal surface moisture fluctuations were almost 180 degrees out of phase with both the tide and the other beach zones. Rather, in this zone moisture fluctuations corresponded closely to potential evaporation rates as shown in the pan measurements (Fig. 9b). The dry zone consistently experienced decreasing moisture contents during the day as evaporation rates increased, and reached minimum moisture contents during or shortly after the period of maximum evaporation rates in the late afternoon. Dry zone moisture contents increased during the night, as measured evaporation rates dropped to about zero. Given that the water table was generally falling in this zone during the night, it is not a plausible source of moisture contributions to the surface sediment, and we therefore interpret this finding to indicate the occurrence of condensation in the surface sediments. This interpretation is supported by the fact that condensation was directly measured in the evaporation pan (i.e., negative evaporation rates) on every night except one. Further, it is probable that the sediment surface cooled more rapidly and to a lower temperature than the pan water during the night (due to the much smaller specific heat capacity of the sediment), which would encourage larger amounts of condensation than that observed in the pan. This finding corresponds well with the evaporation-condensation dynamics outlined for a dry soil layer by Yamanaka et al., (1997, 1998) and Yamanaka and Yonetani (1999).

3.2.3. Non-linear capillary transport: Hysteresis and time lags

The field data clearly demonstrate that groundwater dynamics are the dominant control of surface moisture content in both the wet and variable moisture zones. During the study period, this portion of the beach experienced a number of wetting and drying capillary water flow cycles driven by the oscillations of the water table, which are known to induce a non-linear hysteresis signal on moisture retention in the soil column (Hinz, 1998; Lehmann et al., 1998; Nielsen and Perrochet, 2000; Stauffer and Kinzelbach, 2001; Werner and Lockington, 2003; Cartwright et al., 2005; Cartwright et al., 2009, Schmutz and Namikas, 2013; Cartwright, 2014; Ogden et al. 2015). First described by Haines (1930), this hysteresis results in a disparity between the moisture retention curves of wetting and drying sequences at the same pressure head.

Early hysteresis studies investigated moisture content changes primarily during full drying or wetting cycles (e.g., Childs and Poulovassilis, 1962; Poulovassilis, 1962; Childs, 1969; Raats and Gardner, 1974; Kessler and Rubin, 1987). In natural systems, however, partial drying and wetting water flow cycles are more common, producing what are known as scanning loops – moisture content cycles that occupy a limited portion of the wetting-drying envelope (Lehmann et al., 1998). An examination of the capillary water flow induced scanning loops (Fig. 10) demonstrates the strength of the non-linear hysteretic signal – the smaller the moisture content range (i.e., tighter loops), the weaker the influence of hysteresis on surface moisture dynamics during that wetting/drying sequence.

Fig. 10 shows the sequence of scanning loops for L4, L6, and L9 separated into the three tidal fluctuation regimes (spring, falling, and neap) and the wind/wave set-up episode that occurred during the study period. The data reveal two notable controls on the hysteresis signal: tidal fluctuation magnitude and pressure head magnitude. With diminishing tidal fluctuation magnitude (spring to neap transition) the range in moisture content decreases for all measurement lines, thus reducing the hysteresis signal. Independent of tidal stage, the moisture content range, and thus hysteresis strength, decreases with increasing water table depth (i.e., pressure head) in the landward direction (L9 to

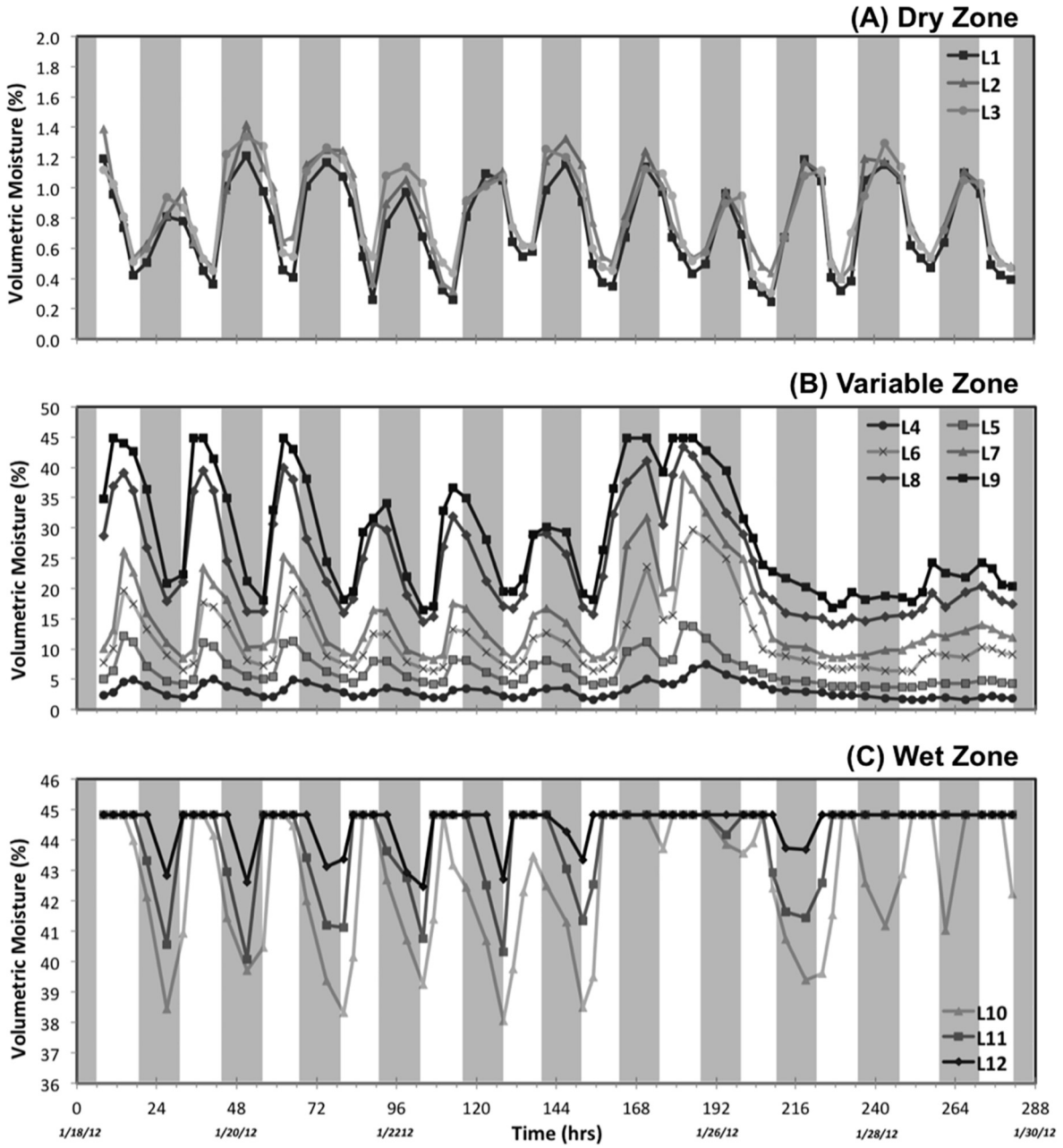

Fig. 7. Time-series of measured surface moisture content at each grid line separated by beach zones: (A) dry zone, (B) variable zone and (C) wet zone. Note the large differences in vertical axis scaling.

L4). Accordingly, the deeper water table at L4 produces a substantially smaller hysteresis signal compared to L9. The wind/wave set-up episode produces a disruption in the diminishing tidal regime by increasing surface moisture content; however, the impact on hysteresis is the same, with increasing water table depth (i.e., pressure head) the strength in hysteresis decreases.

These findings illustrate that hysteresis may have a large effect on spatiotemporal variability in surface moisture. Spatially, variability in moisture content will decrease moving landwards from the berm crest as the depth of the water table increases. However, this spatial pattern is altered in correspondence with tidal stages, and each of the three beach zones will experience differing levels of impact. Overall, these findings fit with data regarding observed trends in beach surface moisture content (Yang and Davidson-Arnott, 2005; Davidson-Arnott et al., 2005, 2008; Namikas et al., 2010; Brakenhoff, 2015).

In addition to hysteresis, the surface moisture content signal also displays a noticeable temporal lag in relation to the water table cycles. In essence, the maximum/minimum surface moisture levels are not reached until some time after the highest/lowest groundwater levels. Table 1 provides the time lag between the maximum/minimum moisture contents and their associated high and low water table levels for the spring and falling tide periods. The neap period was omitted because clear time lag values could not be identified due to the small groundwater fluctuation range and the relatively coarse surface moisture measurement interval. Three patterns are apparent in the time lag behavior. First, the duration of the lag increased with distance from the shoreline (i.e., water table depth). This is not surprising as it takes time for the tidal signal to propagate inland (Baird et al., 1998, Raubenheimer et al., 1999, Horn et al., 2003; Mao et al., 2006, Zhu, 2007; Li et al., 2012; Liu et al., 2013). Second, the time lags associated with low water table are consistently larger than for the high water table. This further demonstrates the inherent hysteresis in the system,

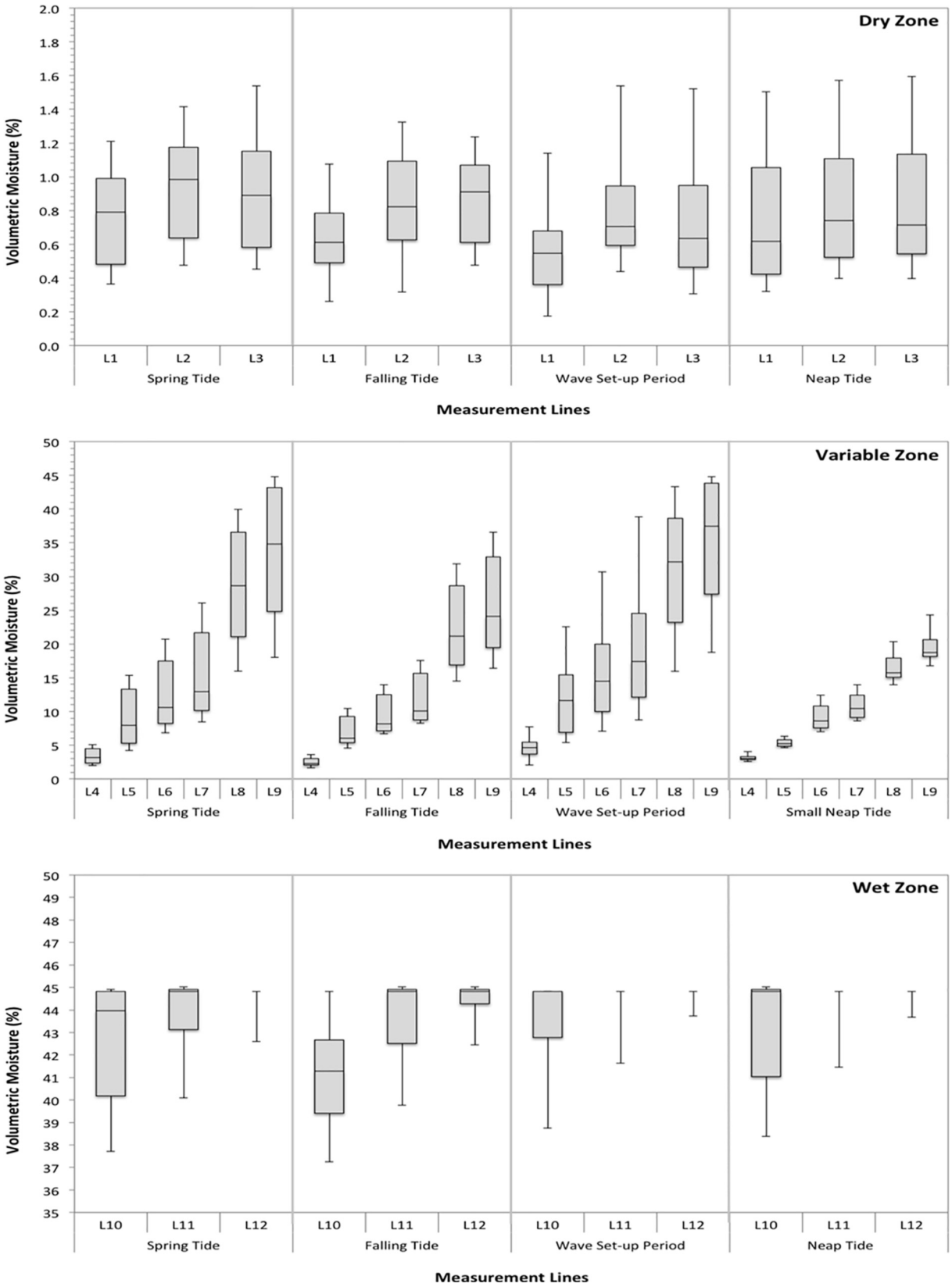

Fig. 8. Box-Whisker plot of surface moisture content for each beach zone (dry, variable, wet) categorized by the four fluctuation regimes (i.e., spring tide, falling tide, wave set-up, and neap tide).

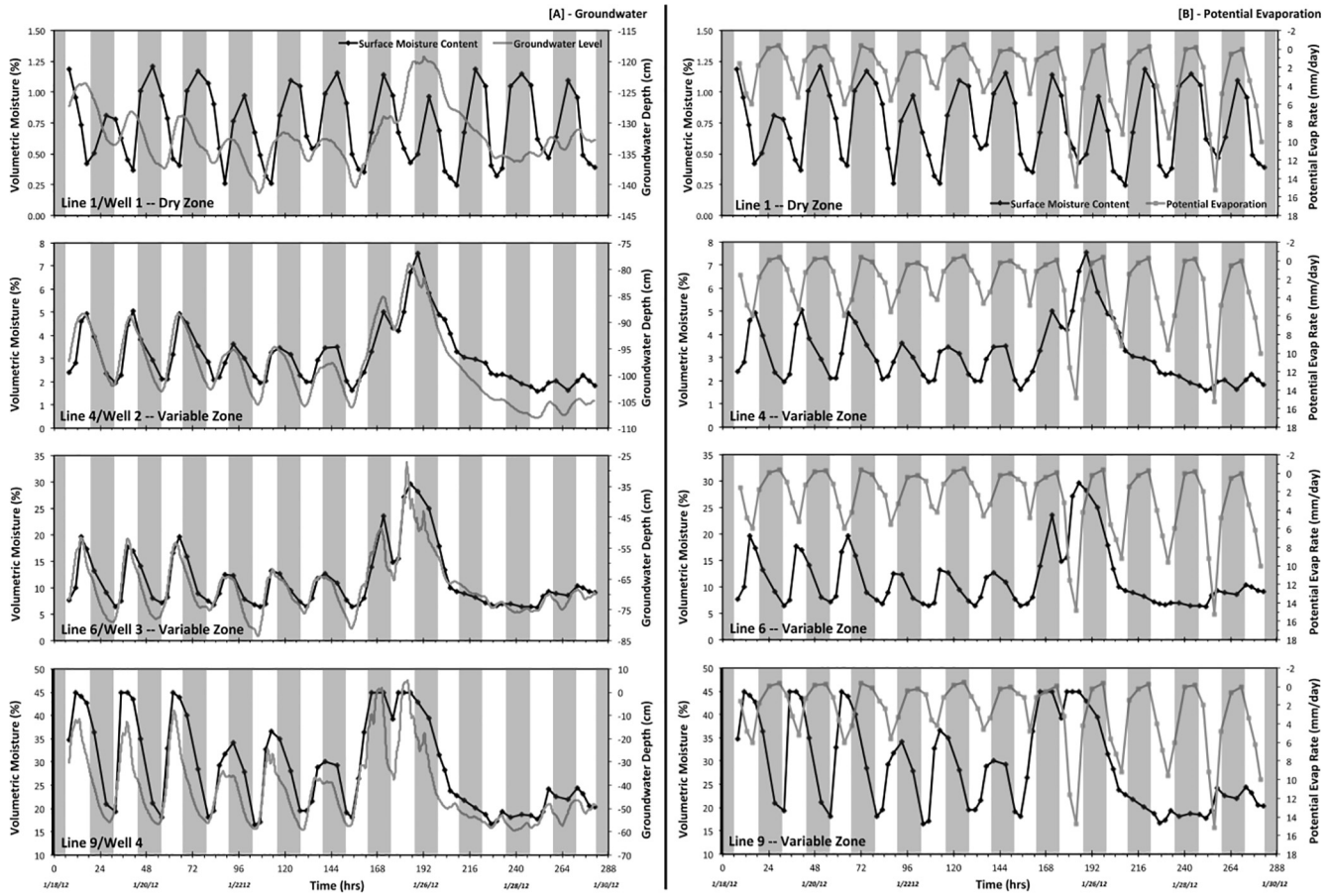

Fig. 9. Time-series of surface moisture at L1, L4, L6, and L9 compared with [A] groundwater elevations at the adjacent wells W1, W2, W3, and W4, and [B] potential evaporation rates.

illustrating that it clearly takes longer for the sediment to drain (reach the lowest surface content) than to fill (reach the maximum content). Finally, the duration of the lag also increased with decreasing tidal range. A number of researchers have established that the hydraulic conductivity of beach sediments is mainly controlled by, and negatively correlated with, the sediment pressure head; an increase in pressure head results in a decrease in hydraulic conductivity (Nielson, 1990; Raubenheimer et al., 1999; Mao et al., 2006). The smaller tidal ranges and deeper groundwater levels associated with the falling and neap tidal periods produce larger pressure heads, corresponding with lower decreased hydraulic conductivity and therefore increased time lags.

4. Modeling

Schmutz and Namikas (2013) demonstrated that a high degree of accuracy is attainable in simulations of surface moisture content variability using the HYDRUS-1D capillary flow model, in the context of a laboratory soil column. This section expands on that research to evaluate the model proficiency in the context of the significantly more complex spatiotemporal variability in real beach moisture content, and also extends it to incorporate evaporation and groundwater dynamics.

4.1. Comparison of measured and simulated surface moisture contents

Time series of the simulated moisture content (calculated using the method described earlier) were generated for each line both with and without an evaporation component. The simulated moisture contents are plotted against the measured moisture contents in Fig. 11. It is immediately evident that evaporation is a key control in the dry zone (Lines 1–3/top panels). In this zone the groundwater-only simulations (no-evap label in figure) depart radically from the measured surface moisture contents. The inclusion of evaporation in the model clearly provides significant improvement in the predicted surface moisture contents, in terms of both the magnitude of the fluctuations and the temporal agreement.

It is also evident in Fig. 11 that the water table elevation is the primary control on surface moisture content in the variable zone. The inclusion of evaporation does not significantly modify predicted moisture content values for lines 5–12. Indeed, the simulations with and without evaporation overlap so closely that the two traces cannot be distinguished on the plots. Only at L4, adjacent to the dry zone, does the inclusion of evaporation generate a modest but detectable improvement in agreement with the measured values. The improvement mainly occurs during periods of low water table elevation, when the influence of groundwater will be at its weakest. This line (L4) clearly demarcates the transition from the variable to the dry zone, a point where the influence of evaporation is just beginning to be detectable during times when groundwater inputs are at a minimum.

For the variable content zone the simulations demonstrate good agreement with the measured values, in terms of both magnitude and timing. A small but systematic difference is evident at the seaward-most line (L9), where the model consistently predicts slightly lower surface moisture content values during the drying sequences. Schmutz and Namikas (2013) described a similar finding from the moisture content of a laboratory soil column. In effect, when the modeled water table is high enough that the surface content approaches saturation, the model predicts that soil pores will begin to drain immediately upon the transition to a decreasing water table elevation. However, both the field and laboratory measurements found that a time lag occurs before the draining begins. Schmutz and Namikas (2013) attributed this time lag

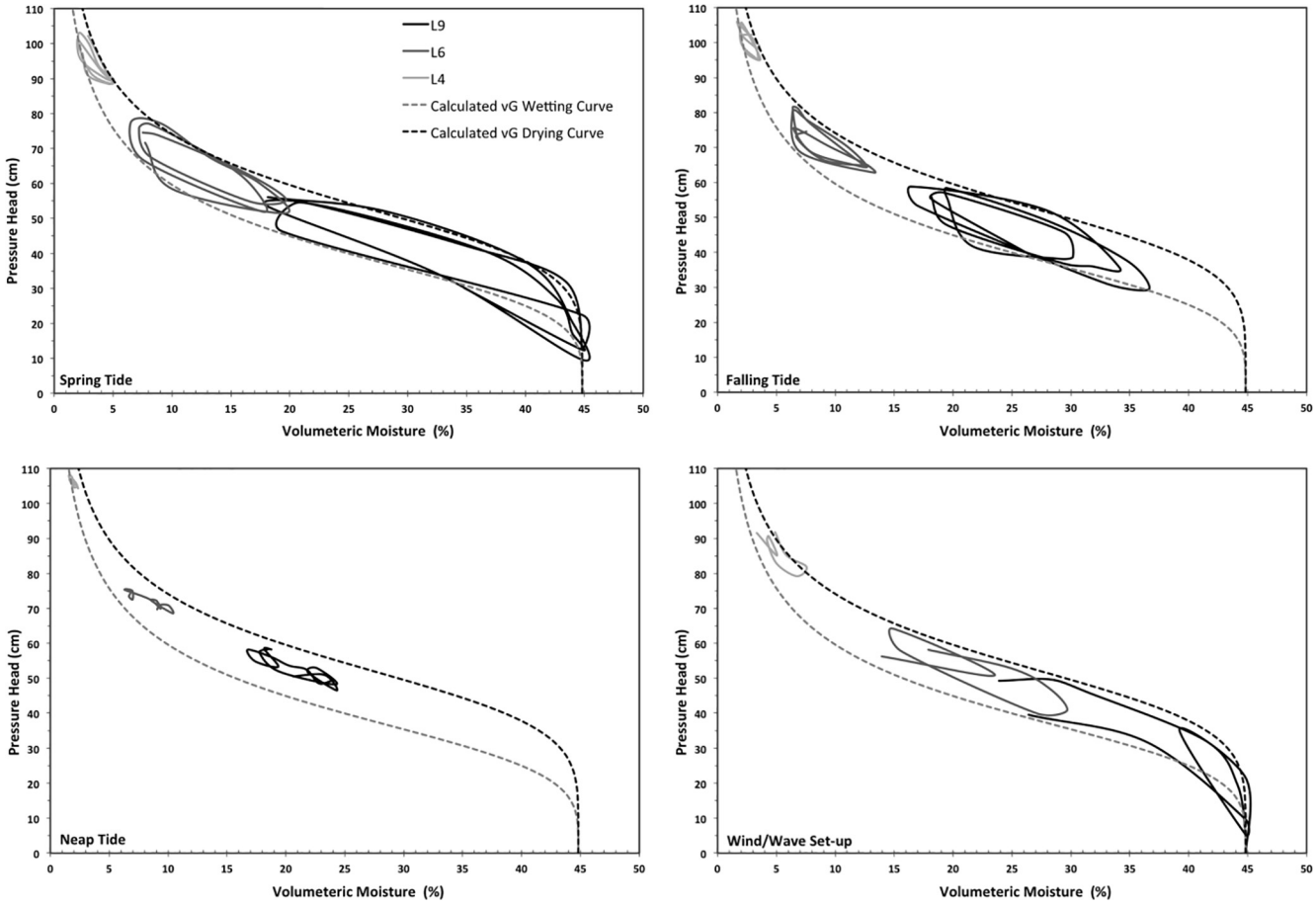

Fig. 10. Water flow-scanning loops for measurement lines L4, L6, and L9 separated by groundwater signals (i.e., spring tide, falling tide, and neap tide) and the wind/wave set-up episode. Also shown are the calculated van Genuchten (1980) boundary wetting and drying curves.

Table 1
Average time lag (hours) between high/low water table levels and max/min surface moisture content for spring and falling tide conditions.

Line	Groundwater Signals			
	Spring		Falling	
	High WT	Low WT	High WT	Low WT
L4	1.5	2.75	2	3.25
L6	0.75	2	1.5	2.25
L9	N/A*	1.25	1	1.5

* Not applicable. In every case the surface content reached saturation before high water due to swash inputs.

to the Haines Jump hysteresis effect (Haines, 1930), or the ink bottle effect, that occurs during the sediment drying process. Haines Jump hysteresis is a function of the soil matric suction required for individual pores drain and fill. During a drying sequence, moisture content remains in the soil pore until the soil matric suction at a particular pressure head becomes too large. At that point the sediment column will abruptly drain. These similar findings in two very different experimental situations demonstrate that the simulation model is not currently able to replicate this effect, and efforts should be made to account for it in future work.

The poorest model fit occurs at the foreshore lines (L10–L12). Here, simulated moisture content matches the measured values well during high water table conditions, but consistently and significantly under predicts during lower water table conditions. This outcome is likely a result of the lack of any consideration of swash inputs in the modeling approach. The model only simulates surface moisture as a result of bottom-up capillary forcing and does not incorporate swash inputs from above, which would supply additional moisture for some time preceding and following high tide. Thus the foreshore lines (L10–L12) experienced larger moisture contents than predicted from groundwater inputs alone. This is clearly another aspect of the beach hydrology system that requires attention in the future. In the context of aeolian processes, however, this particular weakness is relatively unimportant, as the consistently high moisture contents in this zone should preclude significant transport activity.

4.2. Simulated moisture retention curves: Evaporation vs water table

The influence of evaporation versus groundwater on surface moisture can be further clarified by examining the influence of evaporation on moisture retention curves generated from the simulated dataset (Fig. 12). The critical pressure head values above which evaporation begins to impose an influence are about 100 cm during a drying sequence and 90 cm during a wetting sequence. These pressure heads occur at a surface moisture content of approximately 3% by volume in both cases. When the pressure head is below these thresholds, the effect of evaporation on the surface layer is overwhelmed by the input of moisture input via capillary suction from the water table.

This finding has important implications regarding spatiotemporal variability in aeolian transport activity. Several studies have found that surface moisture contents greater than 3% can severely or even completely retard aeolian transport (McKenna Neuman and Nickling, 1989; Sherman et al., 1998; McKenna Neuman and Langston, 2003; Cornelis et al. 2004; Wiggs et al., 2004a,b; McKenna Neuman and Langston,

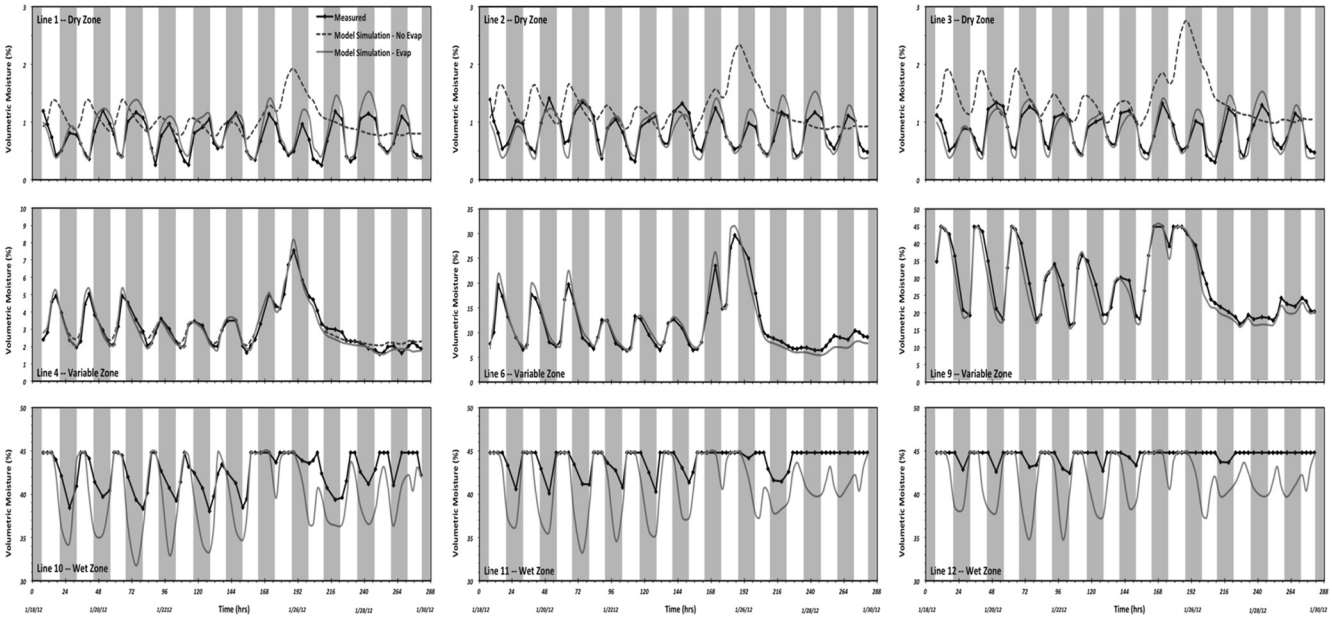

Fig. 11. Time-series of measured and simulated surface moisture contents both with and without evaporation. For lines 5–12 the two simulation results are virtually identical and cannot be distinguished.

2006). It therefore follows that aeolian transport on a given beach would be largely restricted to the dry zone, and possibly the landward most portion of the variable zone. The delineation of this zone should thus allow for estimation and modeling of the potential fetch available to generate transport (Bauer and Davidson-Arnott, 2002; Delgado-Fernandez, 2010). This finding also signifies the importance of surface drying for aeolian transport initiation (Jackson and Nordstrom, 1997; Gillette, 1999; Davidson-Arnott et al., 2005; Baas and Sherman, 2006; McKenna Neuman and Langston, 2006).

4.3. Simulation error evaluation

A quantitative evaluation of the model simulations is given in Fig. 13. It can be seen that the magnitude of the standard error is quite small in the dry zone (L1-L3), where it is typically less than ± 0.2% (water content by volume). This is highly encouraging from the perspective of aeolian transport modeling. Many models of the influence of moisture on transport show large differences in the magnitude of the effect across quite small moisture content ranges (Namikas and Sherman, 1995; Cornelis and Gabriels, 2003), thus fairly precise estimates of surface moisture content would be needed to reasonably

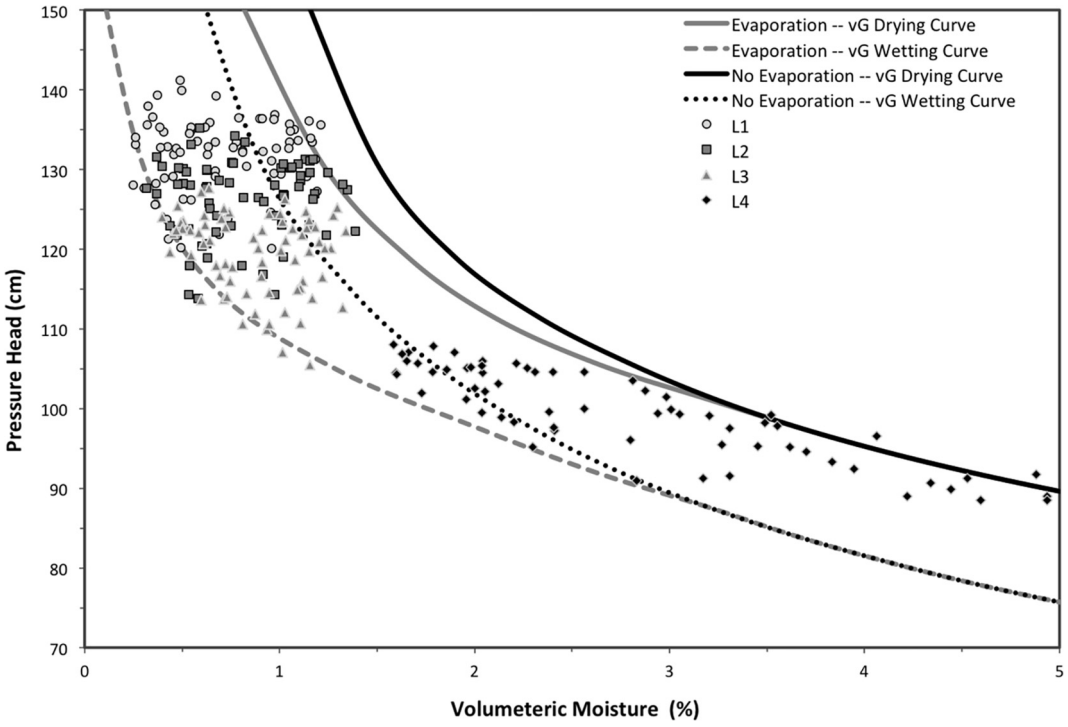

Fig. 12. Simulated moisture retention curves with and without evaporation.

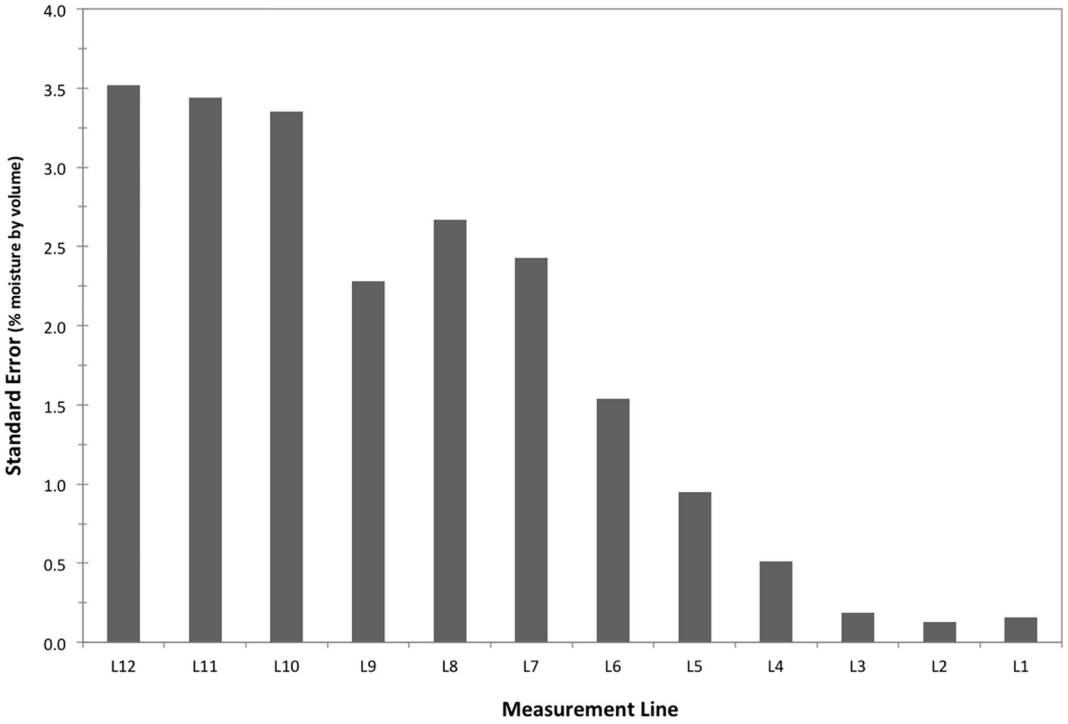

Fig. 13. Absolute standard error in simulated volumetric moisture content for each measurement line.

model the combined system. The prediction error consistently increases moving seaward, reaching a maximum of about ± 3.5% on the upper foreshore. However, the actual moisture contents across most of this zone are large enough that minimal, if any, aeolian transport would be expected.

5. Summary and conclusions

This study documented and modeled spatiotemporal dynamics of beach surface moisture over a twelve-day period. It was found that the spatial pattern could be characterized in terms of three zones. A dry zone of low variability extended 10–15 m seawards of the foredune. Moisture contents in this zone consistently remained under 3%. A variable extended seaward from the dry zone to the berm crest, with moisture contents ranging from about 3% to saturation. The variable zone graded into a wet zone that extended onto the upper foreshore. Moisture contents in the wet zone only rarely fell below 40%, and remained at saturation for extended periods due to swash inputs.

Moisture contents varied over both multi-day and diurnal time scales. Over the longer term, a decrease in both the range and magnitude of moisture content was clearly seen in the variable zone. This trend was associated with the transition from spring to neap tidal conditions. It was temporarily interrupted by an approximately two-day period during which wind and wave setup caused higher water levels that in turn generated increased surface moisture levels and variability. Diurnal cycles in moisture content in the dry zone were seen to be associated with evaporation-condensation cycles. In contrast, diurnal cycles in the variable and wet zones were found to be associated with fluctuating ground water elevations.

Overall, it was found that the spatiotemporal distribution of beach surface moisture is primarily a function of the relative strength of groundwater dynamics (i.e., water table depth and fluctuations) and evaporation-condensation processes. Spatially, the relative strength of the groundwater system weakens moving landward into the back beach where evaporation becomes the primary control on surface moisture content. Temporally, variations in moisture content are associated with the lunar and diurnal tidal cycles and evaporation-condensation signals, as well as the non-linear hysteretic behavior of capillary flows.

Model simulations illustrated that the inclusion of evaporation processes greatly increases the accuracy of simulated surface moisture in the dry zone, where the water table is relatively deep (> 100 cm). In the variable zone, where water table depths are less than 100 cm, evaporation processes did not have a significant influence on surface moisture. Overall, the expanded HYDRUS-1D model employed in this study provides a very reasonable approach to modeling the spatiotemporal variability of beach surface moisture. It was particularly successful in the dry zone, where simulated contents were typically within ± 0.2% of the measured contents. Furthermore, the physical basis of the model makes it broadly applicable as the input parameters can be readily adapted to reflect local beach systems.

This study illustrated a number of important characteristics regarding the nature of spatiotemporal moisture variability, which have direct implications for aeolian processes. It is to be expected that aeolian transport on a given beach will be largely if not completely restricted in space to the dry zone. The delineation of this zone was shown to correspond with the transition from the groundwater system acting as the primary control on surface moisture content to evaporation/condensation processes exerting the primary control. Demarcation of the spatial extent of this zone thus provides the potential fetch available to generate transport activity. Within this zone evaporative drying and condensation inputs exert the dominant control on the potential for initiation of aeolian transport. At the study site this zone was limited to a spatial extent extending about 10–15 m seaward of the foredune toe. However, depending upon local beach characteristics (i.e., grain size, tidal range, beach slope, etc.) it is to be expected that the spatial extent of this zone will vary. The high level of accuracy of the surface content simulations in the dry zone is encouraging although confidence in model performance given different beach characteristics remains to be established.

6. Author statement of contribution

Phillip P. Schmutz: Conceptualization, Methodology, Software, Validation, Formal Analysis, Investigation, Data Curation, Writing –

Original Draft, Visualization, Funding Acquisition. **Steven L. Namikas**: Conceptualization, Methodology, Resources, Writing – Review & Editing, Supervision, Project Administration

Acknowledgements

The authors would like to thank the staff and park rangers at Padre Island National Seashore, especially Wade Stablein, for their helpfulness and courtesy during our time conducting the field research. We would also like to extend thanks to Dr. Brandon Edwards and Dr. Katherine Renken for their invaluable help in the field, as well as their input on early drafts of the manuscript. This study was supported in part by a Doctoral Dissertation Research Improvement (DDRI) Grant, from the Geography and Spatial Sciences (GSS) Program of the National Science Foundation (NFS) (Award #: 1102650).

Appendix A. Supplementary data

Supplementary data associated with this article can be found, in the online version, at https://doi.org/10.1016/j.aeolia.2018.08.001.

References

Aagaard, T., Davidson-Arnott, R., Greenwood, B., Nielsen, J., 2004. Sediment supply from shoreface to dunes: linking sediment transport measurements and long-term morphological evolution. Geomorphology 60 (1–2), 205–224. https://doi.org/10.1016/j.geomorph.2003.08.002.

Abu-Hamdeh, N.H., 2003. Thermal properties of soils as affected by density and water content. Biosyst. Eng. 86 (1), 97–102. https://doi.org/10.1016/S1537-5110(03)00112-0.

Atherton, R.J., Baird, A.J., Wiggs, G.F.S., 2001. Inter-tidal dynamics of surface moisture content on a meso-tidal beach. J. Coastal Res. 17, 482–489.

Aydin, M., Yang, S.L., Kurt, N., Yano, T., 2005. Test of a simple model for estimating evaporation from bare soils in different environments. Ecol. Model. 182, 91–105. https://doi.org/10.1016/j.ecolmodel.2004.07.013.

Baas, A.C.W., Sherman, D.J., 2006. Spatiotemporal variability of aeolian sand transport in a coastal dune environment. J. Coastal Res. 22, 1198–1205. https://doi.org/10.2112/06-0002.1.

Baird, A.J., Mason, T., Horn, D.P., 1998. Validation of a Boussinesq model of beach ground water behavior. Mar. Geol. 148, 55–69. https://doi.org/10.1016/S0025-3227(98)00026-7.

Baird, A.J., Horn, D.P., 2006. Monitoring and modelling groundwater behaviour sandy beaches. J. Coastal Res. 12 (3), 630–640.

Barrilleaux, T.C., Grace, J.B., 2000. Growth and invasive potential of Sapium sebiferum (Euphorbiaceae) within the coastal prairie region: the effects of soil and moisture regime. Am. J. Bot. 87 (8), 1099–1106. https://doi.org/10.2307/2656646.

Bauer, B.O., Davidson-Arnott, R.G.D., Hesp, P.A., Namikas, S.L., Ollerhead, J., Walker, I.W.J., 2009. Aeolian sediment transport conditions on a beach: Surface moisture, wind fetch, and mean transport rates. Geomorphology 105, 106–116. https://doi.org/10.1016/j.geomorph.2008.02.016.

Bauer, B.O., Davidson-Arnott, R.G.D., 2002. A general framework for modeling sediment supply to coastal dunes including wind angle, beach geometry, and fetch effects. Geomorphology 49, 89–108. https://doi.org/10.1016/S0169-555X(02)00165-4.

Brakenhoff, L., 2015. Interaction of tides, groundwater levels and surface moisture on a sandy beach. MSc Thesis, Earth Surface and Water – Coastal Dynamics and Fluvial Systems, Utrecht University, Utrecht, Netherlands.

Cartwright, N., Nielsen, P., Perrochet, P., 2005. Influence of capillarity on a simple harmonic oscillating water table: Sand column experiments and modeling. Water Resour. Res. 41, W08416. https://doi.org/10.1029/2005WR004023.

Cartwright, N., Nielsen, P., Perrochet, P., 2009. Behavior of a shallow water table under periodic flow conditions. Water Resour. Res. 45, W03416. https://doi.org/10.1029/2008WR007306.

Cartwright, N., 2014. Moisture-pressure dynamics above an oscillating water table. J. Hydrol. 512, 442–446. https://doi.org/10.1016/j.jhydrol.2014.03.024.

Chen, X., Hu, Q., 2004. Groundwater influences on soil moisture and surface evaporation. J. Hydrol. 297, 285–300. https://doi.org/10.1016/j.jhydrol.2004.04.019.

Childs, E.C., Poulovassilis, A., 1962. The moving profile above a moving water table. J. Soil Sci. 13, 272–285. https://doi.org/10.1111/j.1365-2389.1962.tb00707.x.

Childs, E.C., 1969. An Introduction to the Physical Basis of Soil Water Phenomena. John Willey & Sons Ltd, New York, pp. 493p.

Cornelis, W.M., Gabriels, D., 2003. The effect of surface moisture on the entrainment of dune sand by wind: an evaluation of selected models. Sedimentology 50, 771–790. https://doi.org/10.1046/j.1365-3091.2003.00577.x.

Cornelis, W.M., Gabriels, D., Hartmann, R., 2004. A parameterisation for the threshold shear velocity to initiate deflation of dry and wet sediment. Geomorphology 59, 43–51. https://doi.org/10.1016/j.geomorph.2003.09.004.

Davidson-Arnott, R.G.D., MacQuarrie, K., Aagaard, T., 2005. The effect of wind gusts, moisture content and fetch length on sand transport on a beach. Geomorphology 68, 115–129. https://doi.org/10.1016/j.geomorph.2004.04.008.

Davidson-Arnott, R.G.D., Yang, Y., Ollerhead, J., Hesp, P.A., Walker, I.J., 2008. The effects of surface moisture on aeolian sediment transport threshold and mass flux on a beach. Earth Surf. Proc. Land. 33, 55–74. https://doi.org/10.1002/esp.1527.

Delgado-Fernandez, I., 2010. A review of the application of the fetch effect to modelling sand supply to coastal foredunes. J. Aeolian Res. 2, 61–70. https://doi.org/10.1016/j.aeolia.2010.04.001.

de Vries, S., de Vries, J.S.M.V., van Rijn, L.C., Arens, S.M., Ranasinghe, R., 2014. Aeolian sediment transport in supply limited situations. J. Aeolian Res. 12, 75–85. https://doi.org/10.1016/j.aeolia.2013.11.005.

Edwards, B.L., Namikas, S.L., 2015. Characterizing the sediment bed in terms of resistance to motion: Toward an improved model of saltation thresholds for aeolian transport. J. Aeolian Res. 19, 123–128. https://doi.org/10.1016/j.aeolia.2015.10.004.

Famiglietti, J.S., Rudnicki, J.W., Rodell, M., 1998. Variability in surface moisture content along a hillslope transect: Rattlesnake Hill, Texas. J. Hydrol. 210, 259–281. https://doi.org/10.1016/S0022-1694(98)00187-5.

Gillette, D.A., 1999. A qualitative geophysical explanation for "Hot Spot" dust emitting source regions. Contrib. Atmos. Phys. 72, 67–77.

Haehnel, R., Buck, N., Song, A., 2014. Moisture effects on eolian particle entrainment. Environ. Fluid Mech. 14 (1), 135–156. https://doi.org/10.1007/s10652-013-9299-y.

Haines, W., 1930. Studies in the physical properties of soil: V. The hysteresis effect in capillary properties, and the modes of moisture distribution associated therewith. J. Agric. Sci. 20, 97–116. https://doi.org/10.1017/S002185960008864X.

Hesp, P.A., 1991. Ecological processes and plant adaptations on coastal dunes. J. Arid Environ. 21, 165–191.

Hinz, C., 1998. Analysis of unsaturated/saturated water flow near a fluctuating water table. J. Contam. Hydrol. 33, 50–80. https://doi.org/10.1016/S0169-7722(98)00065-5.

Horn, D.P., 2002. Beach groundwater dynamics. Geomorphology 48 (1), 121–146. https://doi.org/10.1016/S0169-555X(02)00178-2.

Horn, D.P., Li, L., Holmes, P., 2003. Measurement and modeling of gravel beach groundwater response to wave run-up. In: Davis, R.A. (Ed.), Proceedings of the International Conference on Coastal Sediments 2003. CD-ROM published by World Scientific Publishing Corp. and East Meets West Productions, Corpus Christi, Texas, USA, pp. 11.

Houser, C., 2009. Synchronization of transport and supply in beach-dune interaction. Prog. Phys. Geogr. 33, 733–746. https://doi.org/10.1177/0309133309350120.

Holmes, R.M., 1961. Estimation of soil moisture content using evaporation data. Proceedings of Hydrology Symposium, No. 2 Evaporation. Queen's Printer, Ottawa, pp. 184-196.

Hoonhout, B.M., de Vries, S., 2016. A process-based model for aeolian sediment transport and spatiotemporal varying sediment availability. J. Geophys. Res. – Earth Sci. 121 (8), 1555–1575. https://doi.org/10.1002/2015JF003692.

Hoonhout, B.M., de Vries, S., 2017. Field measurements on spatial variations in aeolian sediment availability at the Sand Motor mega nourishment. J. Aeolian Res. 24, 93–104. https://doi.org/10.1016/j.aeolia.2016.12.003.

Idso, S.B., Reginato, R.J., Jackson, R.D., Kimball, B.A., Nakayama, F.S., 1974. The three stages of drying of a field soil. Soil Sci. Soc. Am. Proc. 38, 831–837. https://doi.org/10.2136/sssaj1974.03615995003800050037x.

Jackson, N.L., Nordstrom, K.F., 1997. Effects of time-dependent moisture content of surface sediments on aeolian transport rates across a beach, Wildwood, New Jersey, USA. Earth Surf. Proc. Land. 22, 611–622. https://doi.org/10.1002/(SICI)1096-9837(199707)22:7<611::AID-ESP715>3.0.CO;2-1.

Kessler, A., Rubin, H., 1987. Relationships between water infiltration and oil spill migration in sandy soils. J. Hydrol. 91, 197–204. https://doi.org/10.1016/0022-1694(87)90204-6.

Legates, D.R., Mahmood, R., Levia, D.F., DeLiberty, T.L., Quiring, S.M., Houser, C., Nelson, F.E., 2010. Soil moisture: A central and unifying theme in physical geography. Prog. Phys. Geogr. 35 (1), 65–86. https://doi.org/10.1177/0309133310386514.

Lehmann, P., Stauffer, F., Hinz, C., Dury, O., Flühler, H., 1998. Effect of hysteresis on water flow in a sand column with a fluctuating capillary fringe. J. Contam. Hydrol. 33, 81–100. https://doi.org/10.1016/S0169-7722(98)00066-7.

Li, L., Barry, D.A., Stagnitti, F., Parlange, J.Y., Jeng, D.S., 2000. Beach water table fluctuations due to spring–neap tides, moving boundary effects. Adv. Water Resour. 23 (8), 817–824. https://doi.org/10.1016/S0309-1708(00)00017-8.

Li, L., Song-hao, S., Xiao-min, M., 2012. Tidal effects on groundwater dynamics in coastal aquifer under different beach slopes. J. Hydrodyn. 24, 97–106. https://doi.org/10.1016/S1001-6058(11)60223-0.

Liu, Y., Huang, H., Qiu, Z., Fan, J., 2013. Detecting coastline change from satellite images based on beach slope estimation in a tidal flat. Int. J. Appl. Earth Obs. Geoinf. 23, 165–176. https://doi.org/10.1016/j.jag.2012.12.005.

Lynch, K., Jackson, D.W.T., Cooper, 2016. The fetch effect on aeolian sediment transport on a sandy beach: a case study from Magilligan Strand, Northern Ireland. Earth Surf. Proc. Land. 41 (8), 1129–1135. https://doi.org/10.1002/esp.3930.

Mahfouf, J.F., Noilhan, J., 1991. Comparative study of various formations from bare soil using in situ data. J. Appl. Meteorol. 30, 1354–1365. https://doi.org/10.1175/1520-0450(1991) 030<1354:CSOVFO>2.0.CO;2.

Mao, X., Enot, P., Barry, D.A., Li, L., Binley, A., Jeng, D., 2006. Tidal influence on behaviour of a coastal aquifer adjacent to a low-relief estuary. J. Hydrol. 327, 110–127. https://doi.org/10.1016/j.jhydrol.2005.11.030.

McKenna Neuman C.L., Langston, G. 2003. Spatial analysis of surface moisture content on beaches subject to aeolian transport. In: Proceedings of the Canadian Coastal Conference (Kingston, Ontario, Canada): 1-10.

McKenna Neuman, C.L., Langston, G., 2006. Measurement of water content as a control of particle entrainment by wind. Earth Surf. Proc. Land. 31, 303–317. https://doi.org/

10.1002/esp.1245.
McKenna Neuman, C., Nickling, W., 1989. A theoretical and wind-tunnel investigation of the effect of capillary water on the entrainment of sediment by wind. Can. J. Soil Sci. 69, 79–96. https://doi.org/10.4141/cjss89-008.
McLachlan, A., 1989. Water filtration by dissipative beaches. Limnol. Oceanogr. 34 (4), 774–780. https://doi.org/10.4319/lo.1989.34.4.0774.
Miller, E.E., Miller, R.D., 1956. Physical theory for capillary flow phenomena. J. Appl. Phys. 27, 324. https://doi.org/10.1063/1.1722370.
Monteith, J.L., 1965. Evaporation and environment. Symp. Soc. Exp. Biol. 19, 205–234.
Monteith, J.L., 1981. Evaporation and surface temperature. Q. J. R. Meteorolog. Soc. 107, 1–27. https://doi.org/10.1002/qj.49710745102.
Mualem, Y., 1976. A new model for predicting the hydraulic conductivity of unsaturated porous media. Water Resour. Res. 12, 513–522. https://doi.org/10.1029/WR012i003p00513.
Namikas, S.L., Edwards, B.L., Bitton, M.C.A., Booth, J.L., Zhu, Y., 2010. Temporal and spatial variability in the surface moisture content of a fine-grained beach. Geomorphology 114, 303–310. https://doi.org/10.1016/j.geomorph.2009.07.011.
Namikas, S.L., Sherman, D.J., 1995. A review of the effects of surface moisture content on aeolian sand transport. In: Tchakerian, V.P. (Ed.), Desert Aeolian Processes. Chapman and Hall, New York, pp. 269–293.
Nielson, P., 1990. Tidal dynamics of the water table in beaches. Water Resour. Res. 26 (9), 2127–2134. https://doi.org/10.1029/WR026i009p02127.
Nielsen, P., Perrochet, P., 2000. Water table dynamics under capillary fringes: experiments and modeling. Adv. Water Resour. 23, 503–515. https://doi.org/10.1016/S0309-1708(99)00038-X.
Ogden, F.L., Lai, W., Steinke, R.C., Zhu, J., 2015. Validation of finite water-content vadose zone dynamics method using column experiments with a moving water table and applied surface flux. Water Resour. Res. 51, 3108–3125. https://doi.org/10.1002/2014WR016454.
Paralange, M.B., Katul, G.G., 1992. Estimation of the diurnal variation of potential evaporation from a wet bare soil surface. J. Hydrol. 132, 71–89. https://doi.org/10.1016/0022-1694(92)90173-S.
Poortinga, A., Keijsers, J.G.S., Maroulis, J., Visser, S.M., 2014. Measurement uncertainties in quantifying aeolian mass flux: evidence from wind tunnel and field site data. PeerJ 2, e454. https://doi.org/10.7717/peerj.454.
Poulovassilis, A., 1962. Hysteresis of pore water, an application of the concept of independent domains. Soil Sci. 93, 405–412. https://doi.org/10.1097/00010694-196206000-00007.
Raats, P.A.C., Gardner, W.R., 1974. Movement of water in the unsaturated zone near a water table. In: van Scholfgaarde, J. (Ed.), Drainage for Agriculture, Agronomy Series. American Society of Agronomy, Madison, WI (pp. 311-357 and 401-405).
Raubenheimer, B., Guza, R.T., Elgar, S., 1999. Tidal water table fluctuations in a sandy ocean beach. Water Resour. Res. 35, 2313–2320. https://doi.org/10.1029/1999WR900105.
Ritchie, J.T., 1972. Model for predicting evaporation from a row crop with incomplete cover. Water Resour. Res. 8, 1204–1213. https://doi.org/10.1029/WR008i005p01204.
Rotnicka, J., 2013. Aeolian vertical mass flux profiles above dry and moist sandy beach surfaces. Geomorphology 187, 27–37. https://doi.org/10.1016/j.geomorph.2012.12.032.
Schmutz, P.P., Namikas, S.L., 2011. Utility of the delta-T theta probe for obtaining surface moisture measurements from beaches. J. Coastal Res. 27 (3), 478–484. https://doi.org/10.2112/08-1130.1.
Schmutz, P.P., Namikas, S.L., 2013. Measurement and modeling of moisture content above an oscillating water table: implications for beach surface moisture dynamics. Earth Surf. Proc. Land. 38, 1317–1325. https://doi.org/10.1002/esp.3418.
Scott, P.S., Farquhar, G.J., Kouwen, N., 1984. Hysteresis effects on net infiltration. Am. Soc. Agric. Eng. 48, 1006–1010.
Sherman, D.J., Jackson, D.W.T., Namikas, S.L., Wang, J.K., 1998. Wind-blown sand on beaches: an evaluation of models. Geomorphology 22, 113–133. https://doi.org/10.1016/S0169-555X(97)00062-7.
Šimůnek J, Sejna M, van Genuchten MT. 1998. The HYDRUS-1D software package for simulating the movement of water, heat, and multiple solutes in variably saturated media. US Salinity Laboratory, ARS, USDA: Riverside, California.
Stauffer, F., Kinzelbach, W., 2001. Cyclic hysteretic flow in porous medium column: model, experiment, and simulations. J. Hydrol. 240, 264–275. https://doi.org/10.1016/S0022-1694(00)00382-6.
Tsegaye, T.D., Tadesse, W., Coleman, T.L., Jackson, T.J., Tewolde, H., 2004. Calibration and modification of impedance probe for near surface soil moisture measurements. Can. J. Soil Sci. 84, 237–243. https://doi.org/10.4141/S03-069.
van Genuchten, M.T., 1980. A closed-form equation for predicting the hydraulic conductivity of unsaturated soils. Soil Sci. Soc. Am. J. 44, 892–898. https://doi.org/10.2136/sssaj1980.03615995004400050002x.
Vicinanza, D., Guida, A., Ferrante, V., Ciavola, P., 2010. Performance of a beach dewatering system – Chiaiolella Beach, Procida Island, Italy. J. Coastal Res. 26 (4), 753–761. https://doi.org/10.2112/08-1165.1.
Vogel, T., Huang, K., Zhang, R., van Genuchten, M.T. 1996. The HYDRUS code for simulating one-dimensional water flow, solute transport, and heat movement in variably-saturated media, Version 5.0, Research Report No 140, U.S. Salinity Laboratory, USDA, ARS, Riverside, CA.
Weise, B.R., White, W.A. 1991. Padre Island National Seashore: A guide to the geology, natural environments, and history of a Texas barrier island. Texas Bureau of Economic Geology, Guidebook 17.
Werner, A.D., Lockington, D.A., 2003. Influence of hysteresis on tidal capillary fringe dynamics in a well-sorted sand. Adv. Water Resour. 26, 1199–1204. https://doi.org/10.1016/S0309-1708(03)00107-6.
Wiggs, C.F.S., Atherton, R.J., Baird, A.J., 2004a. Thresholds of aeolian sand transport: establishing suitable values. Sedimentology 51, 95–108. https://doi.org/10.1046/j.1365-3091.2003.00613.x.
Wiggs, C.F.S., Baird, A.J., Atherton, R.J., 2004b. The dynamic effects of moisture on the entrainment and transport of sand by wind. Geomorphology 59, 13–30. https://doi.org/10.1016/j.geomorph.2003.09.002.
Wilson, G.W., Fredlund, D.G., Barbour, S.L., 1997. The effect of soil suction on evaporative fluxes from soil surfaces. Can. Geotech. J. 34, 145–155. https://doi.org/10.1139/t96-078.
Yamanaka, T., Takeda, A., Sugita, F., 1997. A modified surface resistance approach for representing bare-soil evaporation: wind-tunnel experiments under various atmospheric conditions. Water Resour. Res. 33, 2117–2128. https://doi.org/10.1029/97WR01639.
Yamanaka, T., Takeda, A., Shimada, J., 1998. Evaporation beneath the soil surface: some observational evidences and numerical experiments. Hydrol. Process. 12, 2193–2203. https://doi.org/10.1002/(SICI)1099-1085(19981030)12:13/14<2193::AID-HYP729>3.0.CO;2-P.
Yamanaka, T., Yonetani, T., 1999. Dynamics of the evaporation zone in dry sandy soils. J. Hydrol. 217 (1), 135–148. https://doi.org/10.1016/S0022-1694(99)00021-9.
Yang, Y., Davidson-Arnott, R.G.D., 2005. Rapid measurement of surface moisture content on a beach. J. Coastal Res. 21, 447–452. https://doi.org/10.2112/03-0111.1.
Zhu, Y. 2007. Modeling spatial and temporal variations of surface moisture content and groundwater table fluctuations on a fine-grained beach, Padre Island, Texas. Ph.D. Dissertation, Department of Geography & Anthropology, Louisiana State University: Baton Rouge, Louisiana, US. DOI: etd-08282007-114820.